Published in final edited form as:
Mol Imaging Biol. 2009 ; 11(3): 195–203. doi:10.1007/s11307-008-0181-0.

Toward Quantitative Small Animal Pinhole SPECT: Assessment of Quantitation Accuracy Prior to Image Compensations

Chia-Lin Chen[1], **Yuchuan Wang**[2], **Jason J. S. Lee**[3], and **Benjamin M. W. Tsui**[2]

[1]Department of Medical Imaging and Radiological Sciences, Chung Shan Medical University, Taichung 402, Taiwan, Republic of China

[2]Division of Medical Imaging Physics, The Russell H. Morgan Department of Radiology and Radiological Science, Johns Hopkins University School of Medicine, Baltimore, MD 21287, USA

[3]Department of Biomedical Imaging & Radiological Sciences, National Yang-Ming University, Taipei 102, Taiwan, Republic of China

Abstract

Purpose—We assessed the quantitation accuracy of small animal pinhole single photon emission computed tomography (SPECT) under the current preclinical settings, where image compensations are not routinely applied.

Procedures—The effects of several common image-degrading factors and imaging parameters on quantitation accuracy were evaluated using Monte-Carlo simulation methods. Typical preclinical imaging configurations were modeled, and quantitative analyses were performed based on image reconstructions without compensating for attenuation, scatter, and limited system resolution.

Results—Using mouse-sized phantom studies as examples, attenuation effects alone degraded quantitation accuracy by up to −18% (Tc-99m or In-111) or −41% (I-125). The inclusion of scatter effects changed the above numbers to −12% (Tc-99m or In-111) and −21% (I-125), respectively, indicating the significance of scatter in quantitative I-125 imaging. Region-of-interest (ROI) definitions have greater impacts on regional quantitation accuracy for small sphere sources as compared to attenuation and scatter effects. For the same ROI, SPECT acquisitions using pinhole apertures of different sizes could significantly affect the outcome, whereas the use of different radii-of-rotation yielded negligible differences in quantitation accuracy for the imaging configurations simulated.

Conclusions—We have systematically quantified the influence of several factors affecting the quantitation accuracy of small animal pinhole SPECT. In order to consistently achieve accurate quantitation within 5% of the truth, comprehensive image compensation methods are needed.

Keywords

Quantitation; Pinhole SPECT; Small animal imaging; Image compensations; Attenuation; Scatter; Image resolution

Correspondence to: Benjamin M. W. Tsui; btsui1@jhmi.edu.

Significance: We assessed the quantitation accuracy of small animal pinhole SPECT, providing reference information for the current preclinical studies.

Introduction

Molecular imaging of small animals (e.g., mice and rats) has established a prominent position in many fields of study, such as biology, medicine, and pharmaceutical development [1–3]. Single photon emission computed tomography (SPECT) is an important nuclear medicine imaging modality and a natural and integral component of molecular imaging [4, 5]. For SPECT imaging of small animals (i.e., rodents), a properly designed pinhole collimator can provide a much improved resolution-sensitivity trade-off as compared to other types of collimators [4, 5]. As the number and variety of molecular imaging studies that require the use of pinhole SPECT imaging increase, the need for accurate quantitation under such imaging configurations has also become imperative [6–9]. The goal of this work is to quantify the effects of important factors (e.g., attenuation, scatter, limited system resolution) on quantitation accuracy in the absence of the use of compensation methods through Monte-Carlo simulation methods.

Over the years, significant knowledge has been accumulated for quantitative SPECT imaging in clinical settings, particularly on the importance and effectiveness of compensating for factors that significantly degrade quantitation accuracy in SPECT, e.g., photon attenuation and scatter, and collimator-detector blur [10, 11]. While this knowledge and the proposed compensation methods may be used to facilitate quantitative preclinical SPECT, some unique characteristics of small animal SPECT imaging, such as the routine use of pinhole collimators (as compared to parallel-hole collimators in clinical imaging) and the vastly smaller size of rodents (as compared to human), are expected to make a difference in terms of how one may approach the problem. For example, there have been recent efforts implementing attenuation correction methods for quantitative small animal pinhole SPECT without taking measures to reduce the effects of scatter [12–14]. The scatter effects were deemed negligible, especially in I-125 rodent imaging. Likely due to such arguments, as well as the general preference for having relatively simple data acquisition and processing protocols, comprehensive SPECT image compensations are not routinely applied in current preclinical settings to our knowledge. This state of quantitative small animal pinhole SPECT imaging makes the assessment of quantitation accuracy prior to image compensations very important.

The importance is twofold. First, a systematic assessment will provide valuable reference information for the achievable quantitation accuracy in practice and will guide the design and execution of small animal SPECT imaging protocols. Second, by quantifying how each factor affects quantitation accuracy, one can identify the most influential factors and focus on compensating for them to improve the accuracy or to evaluate, for example, the existing attenuation correction only approach for achieving sufficiently accurate quantitation. Despite the above importance, a comprehensive study of this nature has not been published. This work is intended to fill this void and to facilitate the next stage of quantitative small animal imaging research by systematically assessing the quantitation accuracy prior to image compensations.

There are many factors that can affect the quantitation accuracy in small animal pinhole SPECT, and their influence cannot be separated easily in experimental studies to provide the information needed. The Monte-Carlo simulation (MCS) methods, however, are powerful tools capable of accomplishing this goal. Specifically, we have previously developed and validated an integrated SimSET–GATE MCS workflow that provides fast and realistic simulations of small animal pinhole SPECT systems and can be easily adapted to different imaging system configurations. This workflow will be used to carry out the proposed assessment. Also, to convey the information more clearly and efficiently, we identified and subsequently limited the scope of our discussions to several common factors, selected due to

their relevance to quantitative pinhole SPECT imaging in current practice. Discussions of quantitation are commonly started with well-known physical factors: photon attenuation and scatter inside the small animal. The attenuation and scatter effects are closely associated with other factors such as the isotope used, the size of the rodents (mouse or rat), the location of the sources or the source distribution, and the region-of-interest (ROI) used, all of which were included in this study. For regional quantitation, achievable system resolution is expected to play a role. The choice of pinhole aperture size and radius of rotation (ROR) can affect the achievable system spatial resolution. Therefore, the inclusion of these factors completed the scope of our study.

Materials and Methods

To utilize the MCS workflow for assessing how each of the aforementioned factors would affect the quantitation accuracy, the following steps were employed. First, MCS experiments using phantoms and imaging configurations designed for carrying out a specific investigation were performed to generate simulated SPECT projection data; second, these data were reconstructed using an iterative algorithm without image compensations; finally, data analysis intended for addressing the impact of a specific factor was carried out on the reconstructed images. These steps are detailed in the following.

Simulation Setup

Monte-Carlo Simulation Workflow—Previously, we have developed an efficient MCS workflow [15] by seamlessly integrating the SimSET (simulation system for emission tomography) [16] and the GATE [17] MCS software codes. Specifically, we retained the strength of GATE in describing complex collimator/detector configurations to meet the anticipated future needs for studying advanced pinhole collimation (e.g., multipinhole) geometry while inserting the fast SimSET photon history generator to circumvent the relatively slow GEANT4 MCS code used by GATE in simulating photon transport and interactions inside voxelized phantoms. Significant computational speedup (up to ten times) was achieved with this combination as compared to using the GATE MCS code alone. The use of this workflow facilitated the goal of achieving accurate assessments for each factor in this study, as we were able to efficiently generate realistic and near noise-free MCS data to minimize the influence of statistical noise, and were also able to separate the primary and the scattered photons recorded in the SimSET history file for individual study. In our study, a total of 300 million photons within the phantom were simulated at each SPECT camera position.

Basic Phantoms and Imaging Configurations—Two fundamental components, a phantom and a pinhole SPECT system with a certain imaging configuration, were designed to investigate a specific aspect for quantitation accuracy.

Specifically, the phantoms were composed of a mouse- or rat-sized cylinder, which can be filled with air or water, and a spherically shaped source with a given size. For different experiments, the spherical source was used as a simple geometric representation of a typical radioactive concentration with a given radioisotope and size that is placed at a specific location inside the cylinder. The cylinder used in this study for investigating quantitation at mouse scale has a 28-mm diameter and a 22-mm height, whereas the one for rat was 50 mm in diameter and 70 mm in height (Fig. 1). The source size used for this study ranged from 0.56 to 10 mm in diameter. This cylindrical phantom with the spherical source insert was set up using the SimSET component of the aforementioned SimSET–GATE MCS workflow.

The photon transport and interactions outside the phantoms and in the pinhole SPECT collimator/detector were simulated using the GATE component. The simulated pinhole

SPECT system was based on the X-SPECT™ (Gamma Medica-Ideas, Inc., Northridge, CA, USA) system installed in the Small Animal Imaging Facility at the Johns Hopkins Medical Institutions. The dual 12.5 cm × 12.5 cm modular SPECT detectors used discretized NaI(Tl) crystals with 1.5-mm × 1.5-mm pixels and 6-mm thickness providing projection images in 83 × 83 matrices. They were fitted with a pair of identical pinhole collimators with a 9-cm focal length. The pinhole aperture sizes ranged from 0.5 to 2 mm in diameter, and the RORs were between 2.0 and 4.5 cm. In all simulations, the central axis of the cylindrical phantom coincided with the axis-of-rotation of the circular pinhole SPECT acquisition geometry, around which 64 projection views were acquired over 360°.

Three different isotopes were used in several MCS experiments. For Tc-99m, 140 keV photons were generated. For I-125, photons with ernergies ranging from27 to 35 keV were generated in proportion according to the decay scheme. For In-111, photons with two different energies, 171 and 245 keV, were used. The reference energy resolutions of the SPECT detector were set to 25.3%, 12.5%, and 12.2% for 27, 140, and 171 keV, respectively. The energy windows used in generating the final simulated projection images were the following: 15–45 keV for I-125, 126–154 keV (20%) for Tc-99m, and finally, 156–190 and 222–271 keV for In-111.

Specific MCS Experiments

Experiment No. 1—A Tc-99m, In-111, or I-125 Spherical Source Placed at the Center of a Mouse- or Rat-Sized Cylinder—From our experience, three radioisotopes, Tc-99m, In-111, and I-125, are often used in preclinical SPECT imaging. The proposed experiments were designed to characterize the attenuation and scatter effects for each of them. For both the mouse and the rat MCS experiments, a spherical source (3.26 mm in diameter) with one of the above isotopes was placed at the center of the corresponding air-or water-filled cylindrical phantom. The “source-in-air” experiment without photon attenuation and scatter effects was employed to provide the calibration factor used in the quantitation estimation procedures. For the pinhole SPECT configurations that emulated mouse and rat imaging, 2.5 and 4.5 cm RORs were simulated, respectively. In both cases, a knife-edge pinhole aperture of 1-mm diameter was used.

Experiment No. 2—A Tc-99m Spherical Source Placed at Various Locations Inside a Mouse- or Rat-Sized Cylinder—This experiment was designed to investigate the quantitation accuracy due to combined attenuation and scatter effects for a spherical source placed at various locations within a mouse- or a rat-sized cylindrical phantom. This and other experiments hereafter were performed using only Tc-99m—the most commonly used SPECT isotope, as the results from other isotopes were expected to follow similar trends and can be similarly obtained. For this experiment, the axis-of-rotation (AOR) coincided with the central axis of the cylindrical phantom. First, the spherical source was only moved from the phantom center to different distances from the AOR. The simulation was then repeated with the source located in a plane 6.5 mm from the central plane of the phantom. The size of the spherical source and all other aspects of the image acquisition design were the same as in experiment no. 1, including the source-in-air experiments where the calibration factors were obtained.

Experiment No. 3—A Tc-99m Spherical Source of Various Sizes Placed at the Center of a Mouse-Sized Cylinder—This experiment was designed to assess the influences of source size on the quantitation accuracy. For example, a large source size can introduce quantitation errors due to self-absorption, and for different source sizes, ROI definitions were expected to have varying degrees of impact on quantitation accuracy due to the spatial resolution of the imaging system. In this experiment, a Tc-99m spherical source

with an inner diameter of 0.56, 1, 3.26, or 10 mm was placed at the center of the mouse-sized cylindrical phantom. Other aspects of the imaging acquisition design were the same as those used in experiment no. 1. The results obtained from the smallest sphere (0.56-mm inner diameter) served as the calibration factor for imaging with the larger ones.

Experiment No. 4—A Tc-99m Spherical Source at the Center of a Mouse-Sized Cylindrical Phantom and Imaged with Various Pinhole Aperture Sizes—This experiment was designed to evaluate the effects of pinhole aperture size, which was expected to affect achievable image resolution of the pinhole SPECT system, and therefore, the quantitation accuracy of smaller ROIs. Three pinhole aperture sizes, 0.5, 1, and 2 mm in diameter, were simulated for imaging a Tc-99m spherical source at the center of the mouse-sized cylindrical phantom filled with either air or water. Other imaging parameters were the same as in experiment no. 1.

Experiment No. 5—A Tc-99m Spherical Source at the Center of a Mouse-Sized Cylinder and Imaged with Various RORs—When designing small animal imaging protocols, one may change the ROR to accommodate different rodent sizes and/or to provide different field-of-views. Different RORs were expected to alter the SPECT imaging resolution, as well as the scatter-to-primary-ratio (SPR) in the detected photons due to the change in overall pinhole SPECT geometry. This experiment was designed to investigate the effects of the above alterations on quantitation accuracy. The phantoms (both the spherical source and the cylindrical phantom) and experimental designs were similar to experiment no. 4, except that the pinhole aperture size was fixed at 1 mm, and the ROR of SPECT data acquisitions was set to 2, 2.5, 3, 3.5, and 4.5 cm, respectively, for comparison.

Image Reconstructions

The projection data generated in the above MCS experiments were reconstructed using a 3D iterative OS-EM algorithm [18]. Four subsets with 16 projections per subset were used, and no attenuation, scatter, or collimator-detector response compensations were performed. The reconstructed images, which were saved after each iteration up to a total of ten iterations, were 80×80×80 in matrix size and 0.3 mm in voxel size.

An important factor that must be taken into consideration for pinhole SPECT image reconstructions is the angular dependency and distance dependency of a pinhole collimator's photon detection efficiency (sensitivity). Unlike parallel-hole collimators, the detection efficiency of a pinhole collimator/aperture decreases from the central axis of the collimator. For this reason, the standard calibration procedure for quantitative parallel-hole SPECT does not apply to quantitative pinhole SPECT. Here, additional information such as the precise location of the source and the exact angular dependency and distance dependency for the particular pinhole collimator, are required. Although analytically derived formulas are available to predict the above dependencies, in practice, their accuracy is affected by factors such as photon penetration through the edge of the pinhole aperture and discrepancies between the given and actual design parameters of the pinhole collimator/aperture. Experimental procedures are therefore needed to obtain this information for use in pinhole SPECT image reconstruction. In our MCS study, we performed the point-source-in-air simulation at each of the locations described in our experimental designs to provide the calibration factor for the subsequent source-in-water experiments.

Data Analysis

In order to summarize the findings regarding quantitation accuracy obtained from the MCS experiments more clearly, data analysis using reconstructed images were grouped into two categories.

General Quantitation Accuracy Without Attenuation and Scatter Compensations—In this category, where a single radioactive source (no background activity and adjacent sources) was used, the entire reconstructed image volume was used for quantitative analysis. The effects of blurring due to limited system resolution or low reconstruction iteration numbers are therefore excluded, leaving only the effects of photon attenuation and scatter for the mouse- or rat-sized cylindrical phantom. This approach was applied to all five previously described MCS experiments for studying the general quantitation accuracy under the attenuation and scatter effects in various phantom and system configurations. The general quantitation accuracy was considered as a reference for the subsequent regional analysis, which was used by the MCS experiments no. 3, 4, and 5.

The steps for assessing general quantitation accuracy are as follows. First, the projection data from the source-in-air experiment were reconstructed, and the total pixel intensity gray value summed over the reconstructed image, defined as G_{air}, was recorded. Next, the source-in-water projection data acquired under the same configuration were reconstructed, and a value of G_{wat} was similarly obtained. Since the total number of simulated photons originating from the radioactive source were identical for both in-air and in-water experiments, the quantitation accuracy for the in-water case was therefore degraded by $(G_{wat}-G_{air})/G_{air} \times 100\%$. This degradation (or quantitation error) can be attributed to the combination of attenuation and scatter effects in the water-filled phantom. As mentioned previously, the use of the MCS workflow allowed separation of primary and scattered photons (e.g., through identifying event flags in the MCS process); therefore, if the scattered photons were not included in the projection data, the resulting degradation calculated for G_{wat} would solely characterize the effect of photon attenuation. The sole effect of scatter could be similarly determined.

Specifically for experiment no. 3, in order to examine the effect of self-absorption due to large source size, the following steps were used. First, G_{air}' was obtained from the experiment using the smallest spherical source (0.56 mm). Next, each of the larger spherical source Gair′ was obtained. Since the total number of simulated photons originating from the source phantom were identical for all sizes of sphere sources, the quantitation accuracy for the larger sphere source as compared to the smallest sphere was degraded by $(G_{air}'-G_{air})/G_{air} \times 100\%$. This degradation can mostly be attributed to the self-attenuation/absorption in larger sphere sources.

Regional Quantitation Accuracy with Effects of Finite System Resolutions—In preclinical small animal imaging, regional quantitation may be required due to the presence of background and/or adjacent activity. For a given system resolution and iterative reconstruction algorithm, both the number of subsets and the ROI definitions can affect the regional quantitation. This analysis was of particular interest for MCS experiments no. 3, 4, and 5.

Using the source-in-air MCS experiments as examples, the steps for assessing regional quantitation accuracy with respect to number of iterations are as follows. First, the projection data were reconstructed to obtain G_{air}, the total pixel intensity value over the entire reconstructed image that is independent of iteration numbers. Next, at each iteration number, calculate the total pixel intensity value within a predefined ROI in the reconstructed images R_{air}. For the given ROI, the quantitation error was $(R_{air}-G_{air})/G_{air} \times 100\%$. This error will be non-zero if the predefined ROI was not sufficiently large and will converge to a certain value as the iteration number increases. The ROI used in this analysis was defined by the physical spherical source size and location in the simulated phantom.

Similarly, the steps for assessing regional quantitation accuracy with respect to the ROI definitions are as follows. First, obtain G_{air} as above. Next, at a fixed reconstruction iteration number (usually after the aforementioned convergence), R_{air} was obtained based on a different ROI definition each time to calculate the regional quantitation accuracy $R_{air}/G_{air} \times 100\%$. This was used to compute a recovery coefficient for this particular combination of ROI, phantom, and imaging configuration. As the size of the ROI increases, the quantitation accuracy (or recovery coefficients) should approach and eventually reach 100% for source-in-air MCS experiments. In this study, five different ROI definitions were used. The first ROI was strictly defined by the physical spherical source size and location in the simulated phantom; the second ROI was defined by increasing the radius of the first ROI by 0.5 pixel (or 0.15 mm); the third ROI by one pixel (0.3 mm); the fourth and fifth ROIs by 1.5 pixels (0.45 mm) and two pixels (0.6 mm), respectively.

Results

The results of all MCS experiments were summarized based on the data analysis categorization described in the previous section.

General Quantitation Accuracy Without Attenuation and Scatter Compensations

Table 1 compares the quantitation errors from a 3.26-mm inner diameter spherical source filled with three different radioisotopes and placed inside a mouse- and a rat-sized cylindrical phantom obtained from experiment no. 1. The quantitation errors due to uncompensated photon attenuation, scatter, and combined effects were labeled as (A), (S), and (A+S), respectively. As expected, for all three radioisotopes studied, both attenuation and scatter effects are greater in the rat-sized phantom than in the mouse-sized phantom. Notably, quantitation errors for the spherical source at the center of the mouse-sized phantom due to uncompensated attenuation effect are greater for I-125 (−41%) than for Tc-99m or In-111. However, for the same phantom, uncompensated scatter effects result in a 20% degradation in quantitation accuracy for I-125, significantly greater than that for Tc-99m or In-111. With the combined effects, the degradations of quantitation accuracy for Tc-99m or In-111 are shown to be about −12% for mouse and −21% for rat, whereas for I-125, they are about −21% and −37%, respectively.

The results from experiment no. 2 depicting the quantitation error with respect to source location are plotted in Fig. 2. For both mouse- and rat-sized phantoms, the quantitation accuracy without image compensations improves as the source is moving away from the AOR, and a slightly slower rate of improvement is observed when the source is placed away from the central cross-sectional plane of the cylindrical phantom.

From the data obtained in experiment no. 3 and analyzed using the approach discussed in “General quantitation accuracy without attenuation and scatter compensations”, the quantitation errors due to self-attenuation/absorption for larger spherical sources (with respect to the calibration source) are found to be −0.5%, −1.1%, and −3.6% with 1, 3.26, and 5 mm in inner diameters, respectively.

The results of experiment no. 4 show that quantitation errors due to attenuation and scatter effect can be considered as independent of pinhole size. When different pinhole aperture sizes (0.5-, 1-, and 2-mm diameter) are used, the errors are −12.2%, −12.1%, and −12.0%, respectively.

For experiment no. 5, the use of different RORs at 2, 2.5, 3, 3.5, and 4.5 cm shows slight decrease in the general quantitation errors of −12.3%, −12.1%, −11.9%, −11.8%, and

−11.7%, respectively, as caused by the combined attenuation and scatter effects. As stated previously, this is due to the small changes in SPR at different RORs.

Regional Quantitation Accuracy with Effects of Finite System Resolutions

Using the physical size of the spherical source as ROI in experiment no. 3, we observe how the regional quantitation accuracy improves and converges as the iteration number increases (Fig. 3a). For small size spheres, the rate of improvement is slightly slower as compared to that for bigger size spheres. In general, a sufficient number of iterations are required to reach the convergence, where a large regional quantitation error (−77%) is observed for the 0.28-mm spherical source and the ROI used. The larger the sphere source is, the less regional quantitation error at the convergence. By fixing the iteration number at 10, in Fig. 3b, we show that these errors are reduced by using larger ROIs, resulting in improved recovery coefficients. For example, a 0.45-mm (1.5 pixels) increase in ROI size provides a recovery coefficient very close to 1.0 for spheres of all sizes.

By similarly analyzing the data in experiment no. 4, we find that the improvement of regional quantitation accuracy with respect to iteration numbers is significantly faster when a smaller pinhole aperture is used, which also results in less quantitation error at the convergence (Fig. 4a). When the large 2-mm aperture is used, an error of −50% is observed, as compared to −10% for the 0.5-mm aperture at large iteration numbers. With all the larger ROIs we studied, the recovery coefficient for the 2-mm aperture is still significantly lower than 1.0 (Fig. 4b).

Finally, from experiment no. 5, we find that the regional quantitation errors are affected by RORs only at the early iteration numbers (Fig. 5a), where a larger ROR is associated with a slightly greater error. However, given sufficiently large iteration numbers, the error convergence is nearly identical for all RORs. The improvements in the recovery coefficients when the ROI size increases are also similar (Fig. 5b).

Discussion

Based on the above results, the general quantitation accuracy affected by attenuation and scatter effects are closely associated with the isotopes used, the size of the phantom, and the location of the source within the phantom. Self-attenuation/absorption in a large source can also degrade the quantitation accuracy if unaccounted for. The pinhole SPECT system parameters such as pinhole aperture size and ROR only have negligible effects when a sufficiently large ROI is used.

In terms of radioisotopes, the results related to I-125 from experiment no. 1 are contrary to previous claims that scatter effects are negligible for quantitative I-125 small animal pinhole SPECT [14]. We observed a significant fraction of scattered photons during simulated pinhole SPECT data acquisitions using the I-125 source. The previous claims were made based on the fact that the probability for Compton interactions at the lower energy range characterizing I-125 are lower than those of higher energy photons. However, further analysis indicates that for 27–35 keV photons from I-125, the scatter photopeak (contributed by backscatters) is very close to the main photopeak (Fig. 6). Due to the energy resolution and compact nature of the scatter energy spectrum, narrowing the energy windows, which is an effective way of reducing the effects of scatter for Tc-99m SPECT, is no longer viable for I-125 SPECT, resulting in a large amount of scattered photons detected. Based on the results in Table 1, for mouse I-125 pinhole SPECT imaging, performing only attenuation compensation (AC) will shift the quantitation error from −21% (A + S) to 20% (S). In other words, hardly any improvement in quantitation accuracy is obtained. At rat size, due to more

severe attenuation effects, performing only AC can change the error from −37% to 25%, an improvement that might be unsatisfactory in many quantitation tasks.

The results in experiment no. 1, where the spherical sources were placed at the center of a mouse- or rat-sized cylindrical phantom, were useful for providing an estimate on the worst general quantitation accuracy one can expect prior to image compensations, as the accuracy will improve for the off-center locations, as shown in experiment no. 2. This information can be used to guide small animal pinhole SPECT imaging in preclinical settings. Although these MCS studies were based on simple cylindrical phantoms and uniform attenuation media, they were expected to be close approximations of imaging configurations in practice. To demonstrate this, we performed an additional MCS experiment using the realistic digital mouse whole-body phantom (MOBY) [19]. The overall dimensions of the MOBY phantom (28 mm of body long axis, 26.3 mm of short axis, and 22 mm of height) was similar to the cylindrical phantom shown in Fig. 1. A small area of Tc-99m tracer uptake was placed in the aorta region, which is very close to the center of the phantom. With the realistic non-uniform attenuation map provided by MOBY, we find quantitation errors of −17% (A), 5% (S), and −12% (A + S), which are very close to those shown in Table 1.

In preclinical small animal imaging, regional quantitation tasks are often needed. As our results indicated, regional quantitation accuracy can be greatly affected by ROI definition, number of reconstruction iterations, and imaging parameters such as pinhole aperture size. This is especially significant when quantifying a small region (evident in experiment no. 3) with a dimension that is on the order of or smaller than the achievable system resolution, where factors such as ROI definition can have a much greater effect on quantitation accuracy than photon attenuation and scatter. For this reason, while implementations of attenuation and scatter compensations will improve the general quantitation accuracy, a number of other factors must be also considered to achieve accurate regional quantitation.

Based on our results from experiment no. 3, without image compensations to improve the achievable image resolution, whenever possible, a sufficiently large reconstruction iteration number and a ROI larger than the physical size of the source should be used for regional quantitation. When larger ROIs cannot be used for regional quantitation in practice, for example, when quantifying tracer uptake within or near significant background activity or in close proximity to other focal uptakes, image compensation techniques for resolution-recovery (e.g., collimator-detector response compensation) and potentially partial volume correction methods will be very important for achieving high quantitation accuracy on small regions.

For the particular mouse imaging configuration we studied in experiment no. 5, the change in the ROR did not have a significant impact on regional quantitation. On the other hand, as shown in experiment no. 4, a smaller pinhole aperture is favorable for quantifying small regions. However, this conclusion is based on the near noise-free MCS data. In practice, for the same acquisition time, the use of smaller pinhole apertures will introduce a higher level of statistical noise. Statistical noise can greatly affect the precision (but not accuracy) of a quantitation task. The optimum trade-off between resolution and image noise is an important topic in image evaluation for a specific imaging task such as detection and discrimination. Nevertheless, in order to achieve accurate pinhole SPECT quantitation, simultaneous efforts must be made to improve both accuracy and precision. Accuracy can be improved through the use of proper image compensation methods, while precision must be improved with the acquisition of data with low statistical noise. Otherwise, the efforts of improving quantitation accuracy might be negated by poor precision in practice.

Conclusions

We have identified a number of factors and assessed their influence on both general and regional quantitation accuracy in small animal pinhole SPECT. While providing reference information for current preclinical studies, this assessment is useful for justifying the investigation of image compensation methods. Notably, our results indicate that contrary to previous claims, scatter effects must be taken into account to achieve acceptable quantitation accuracy for I-125 imaging, and in order to consistently achieve general quantitation accuracy within 5% of the truth for all the isotopes studied, both attenuation and scatter compensations are required. For regional quantitation accuracy, ROI definitions could have a greater impact than attenuation and scatter effects. To improve regional quantitation accuracy, especially for quantifying a region with a size on the order of or smaller than the achievable system resolution, it is crucial to compensate for the finite system resolution of the pinhole SPECT systems.

Acknowledgments

The authors would like to thank Drs. Eric Frey and Yong Du (Johns Hopkins Univ.) for their valuable suggestions. Special thanks go to Martin Stump for carefully editing the manuscript. This project is partially supported by the US Public Health Service Grants EB168 and EB1558.

References

1. Weissleder R, Mahmood U. Molecular imaging. Radiology. 2001 May.219:316–333. [PubMed: 11323453]
2. Pomper MG. Molecular imaging: an overview. Acad Radiol. 2001 Nov.8:1141–1153. [PubMed: 11721814]
3. Pomper MG. Translational molecular imaging for cancer. Canc Imag. 2005; 5:S16–S26. Spec No A.
4. Beekman F, van der Have F. The pinhole: gateway to ultra-high-resolution three-dimensional radionuclide imaging. Eur J Nucl Med Mol Imaging. 2007 Feb.34:151–161. [PubMed: 17143647]
5. Meikle SR, Kench P, Kassiou M, Banati RB. Small animal SPECT and its place in the matrix of molecular imaging technologies. Phys Med Biol. 2005 Nov 21.50:R45–R61. [PubMed: 16264248]
6. Acton PD, Choi SR, Plossl K, Kung HF. Quantification of dopamine transporters in the mouse brain using ultra-high resolution single-photon emission tomography. Eur J Nucl Med Mol Imaging. 2002 May.29:691–698. [PubMed: 11976810]
7. Acton PD, Thomas D, Zhou R. Quantitative imaging of myocardial infarct in rats with high resolution pinhole SPECT. Int J Cardiovasc Imaging. 2006 Jun.22:429–434. [PubMed: 16518671]
8. Alvarez-Fischer D, Blessmann G, Trosowski C, et al. Quantitative [I-123]FP-CIT pinhole SPECT imaging predicts striatal dopamine levels, but not number of nigral neurons in different mouse models of Parkinson's disease. Neuroimage. 2007 Oct 15.38:5–12. [PubMed: 17716921]
9. Liu ZL, Kastis GA, Stevenson GD, et al. Quantitative analysis of acute myocardial infarct in rat hearts with ischemia–reperfusion using a high-resolution stationary SPECT system. J Nucl Med. 2002 Jul.43:933–939. [PubMed: 12097466]
10. Tsui BMW, Frey EC, Zhao X, Lalush DS, Johnston RE, Mccartney WH. The importance and implementation of accurate 3d compensation methods for quantitative SPECT. Phys Med Biol. 1994 Mar.39:509–530. [PubMed: 15551595]
11. Tsui BMW, Zhao XD, Frey EC, Mccartney WH. Quantitative single-photon emission computed-tomography—basics and clinical considerations. Semin Nucl Med. 1994 Jan.24:38–65. [PubMed: 8122128]
12. Deloar HM, Watabe H, Aoi T, Iida H. Evaluation of penetration and scattering components in conventional pinhole SPECT: phantom studies using Monte Carlo simulation. Phys Med Biol. 2003 Apr 21.48:995–1008. [PubMed: 12741497]
13. Li J, Jaszczak RJ, Coleman RE. Quantitative small field-of-view pinhole spect imaging—initial evaluation. IEEE Trans Nucl Sci. 1995 Aug.42:1109–1113.

14. Hwang AB, Taylor CC, VanBrocklin HF, Dae MW, Hasegawa BH. Attenuation correction of small animal SPECT images acquired with I-125-iodorotenone. IEEE Trans Nucl Sci. 2006 Jun. 53:1213–1220.

15. Chen C-L, Wang Y, Lee JJS, Tsui BMW. Integration of SimSET photon history generator in GATE for efficient Monte Carlo simulations of Pinhole SPECT. Med Phys. 2008 July.35:3278–3284. [PubMed: 18697552]

16. Harrison RL, Haynor DR, Gillispie SB, Vannoy SD, Kaplan MS, Lewellen TK. A public-domain simulation system for emission tomography-photon tracking through heterogeneous attenuation using importance sampling. J Nucl Med. 1993 May.34:P60–P60.

17. Jan S, Santin G, Strul D, et al. GATE: a simulation toolkit for PET and SPECT. Phys Med Biol. 2004 Oct 7.49:4543–4561. [PubMed: 15552416]

18. Wang YC, Tsui BMW. Pinhole SPECT with different data acquisition geometries: Usefulness of unified projection operators in homogeneous coordinates. IEEE Trans Med Imag IEEE. 2007 Mar. 26:298–308.

19. Segars WP, Tsui BMW, Frey EC, Johnson GA, Berr SS. Development of a 4-D digital mouse phantom for molecular imaging research. Mol Imag Biol. 2004 May–Jun.6:149–159.

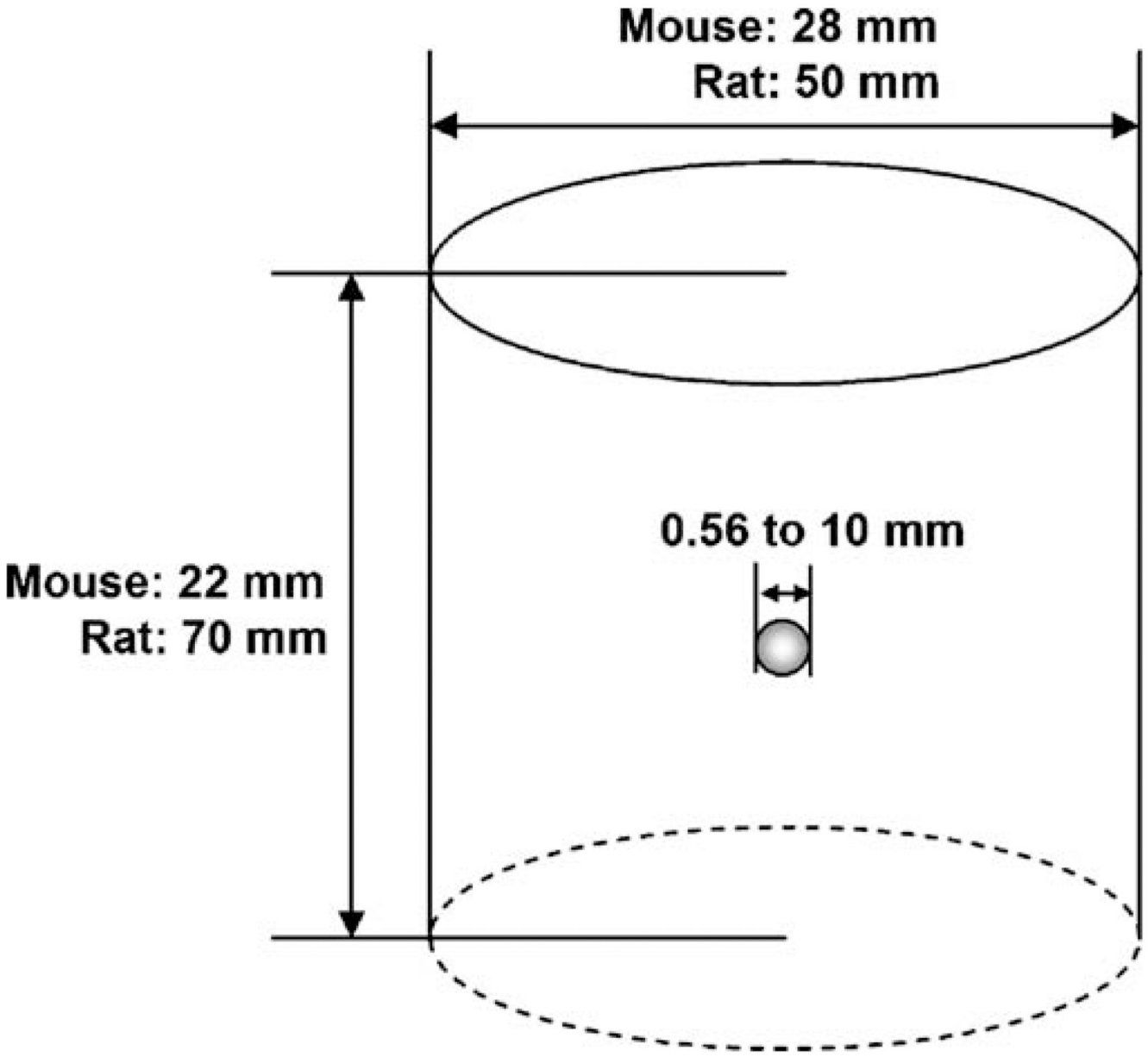

Fig. 1.
The basic phantoms used for the study, including a mouse-/rat-sized cylindrical phantom that can be filled with either air or water and spherical sources of various sizes (a 3.26-mm diameter sphere source was used in experiments 1, 2, 4, and 5).

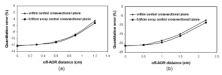

Fig. 2.
Impact of spherical source locations on uncompensated photon attenuation and scatter for pinhole SPECT quantitation accuracy for a Tc-99m spherical source within **a** a mouse-sized phantom and **b** a rat-sized phantom, respectively. The sphere source is at central or off-central cross-sectional plane of the cylindrical phantom and various locations away from AOR.

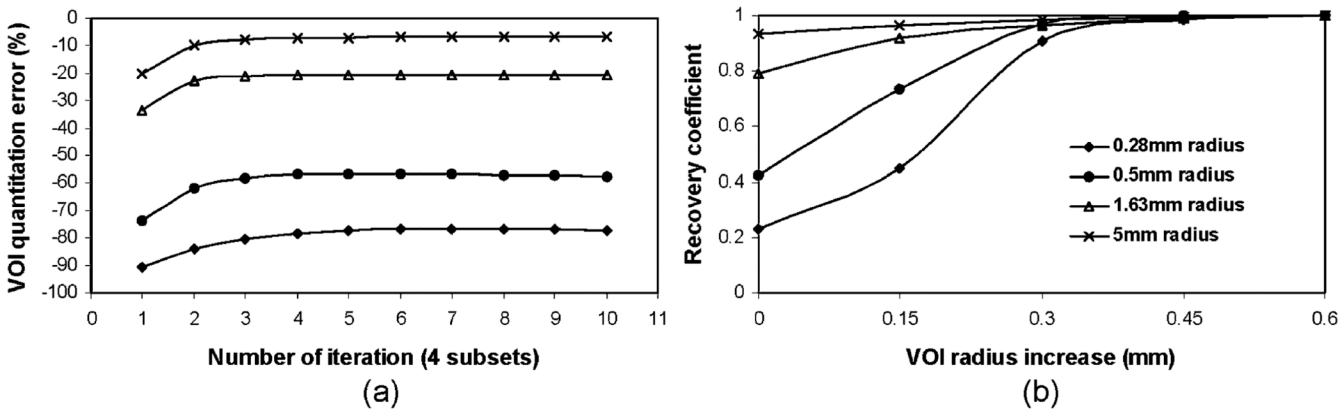

Fig. 3.

Errors of ROI quantitation for Tc-99m spherical source of different sizes. **a** ROI quantitation errors vs. iteration number. ROIs corresponding to the physical size of simulated sphere were used. **b** Recovery coefficient vs. an increase of ROI radius upon physical size using reconstructed images at the tenth iteration.

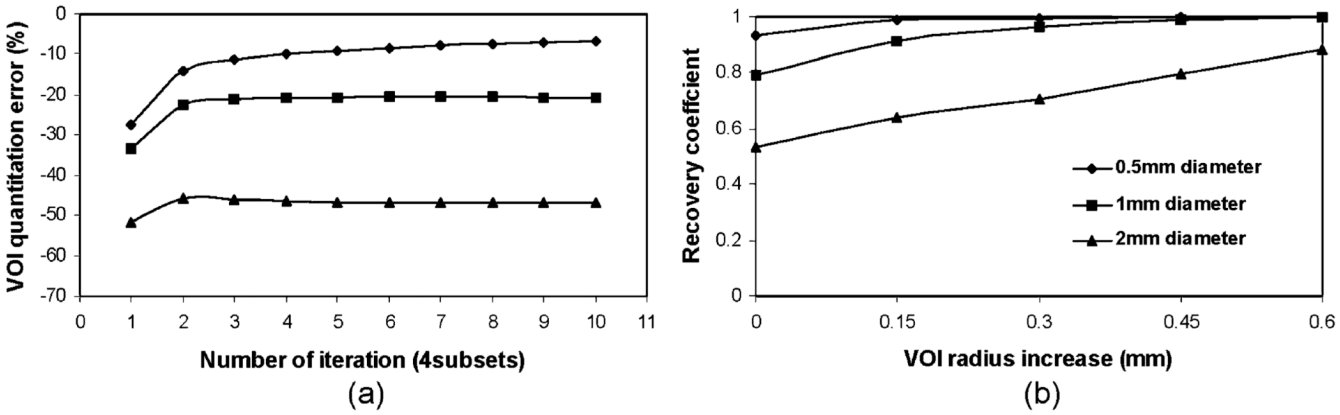

Fig. 4.

Effects of different pinhole aperture sizes (0.5, 1, and 2 mm in diameter) on ROI quantitation. **a** ROI quantitation vs. iteration number. ROIs corresponding to the physical size of simulated Tc-99m sphere are used. **b** Recovery coefficient vs. ROI definition using reconstructed images at tenth iteration.

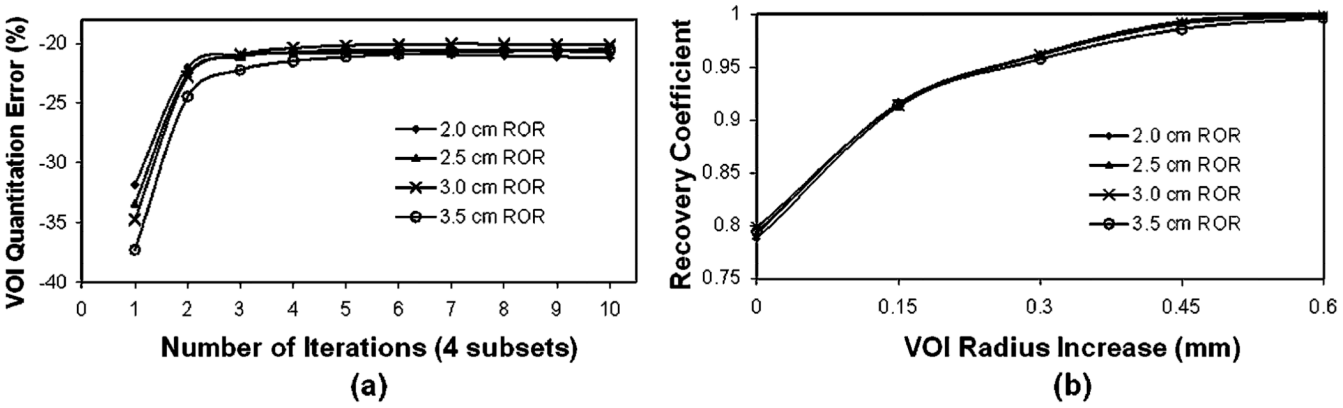

Fig. 5.

Effects of different RORs (2, 2.5, 3, 3.5, and 4.5 cm) on ROI quantitation. **a** ROI quantitation vs. iteration number. ROIs corresponding to the physical size of simulated Tc-99m sphere are used. **b** Recovery coefficient vs. ROI definitions using reconstructed images at tenth iteration.

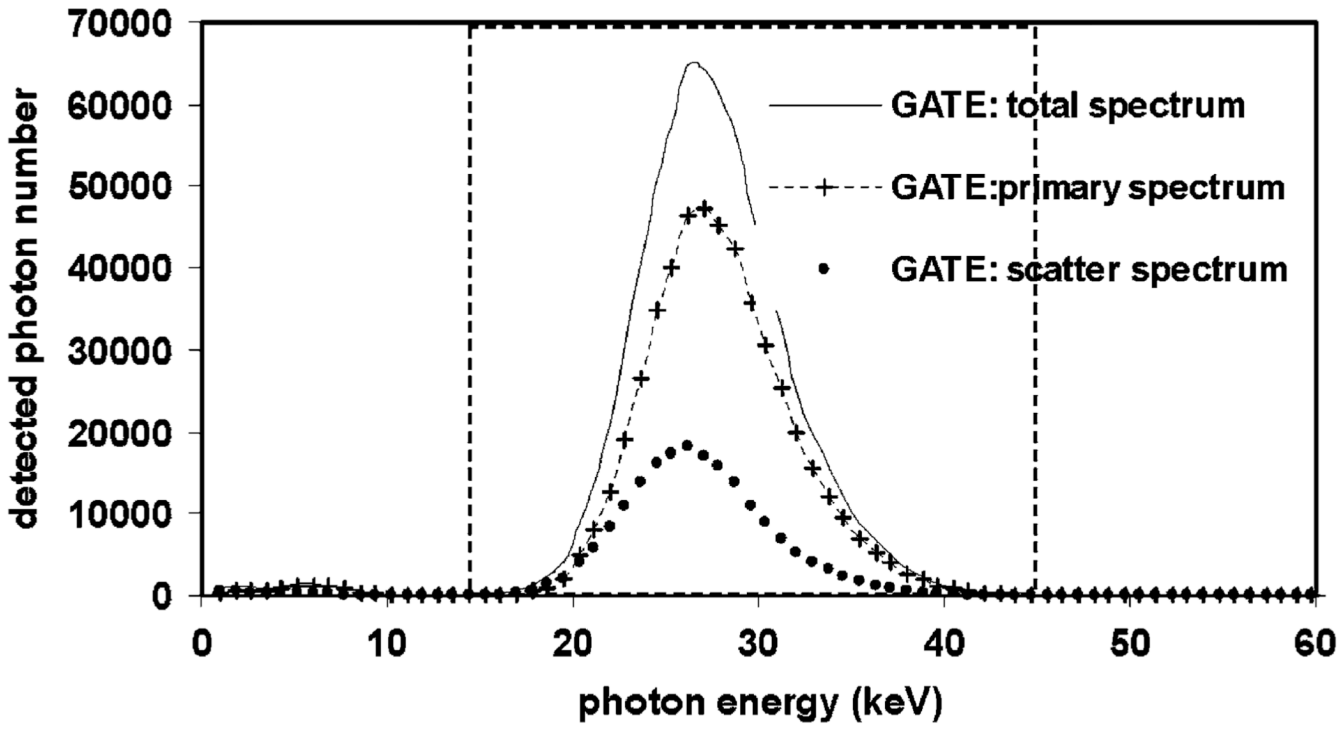

Fig. 6.
The energy spectrum of I-125 pinhole SPECT imaging. The scatter peak is very close to the primary peak, resulting in large percentage of scattered photons being detected.

Table 1

Comparison of quantitation errors in small animal pinhole SPECT due to uncompensated photon attenuation (A), scatter (S), and combined effects (A + S) for a spherical source with 3.26 mm in inner diameter at the center of the water-filled mouse- or rat-sized cylindrical phantom

	Quantitation error (%)								
	I-125			Tc-99m			In-111		
Phantom	A	S	A + S	A	S	A + S	A	S	A + S
Mouse-sized	−41.1	19.6	−21.5	−18.5	6.1	−12.4	−16.6	4.0	−12.6
Rat-sized	−62.7	25.1	−37.6	−30.6	9.1	−21.5	−28.3	6.9	−21.4